EPJ manuscript No.
(will be inserted by the editor)

Controlling and characterising the deposits from polymer droplets containing microparticles and salt

Y. Msambwa, A.S.D. Shackleford, F.Ouali and D.J. Fairhurst

Nottingham Trent University, Clifton Lane, Nottingham, NG11 8NS, UK

Received: date / Revised version: date

Abstract. It is very well known that as suspension droplets evaporate, a pinned contact line leads to strong outwards capillary flow resulting in a robust coffee ring-stain at the periphery of the droplet. Conversely tall pillars are deposited in the centre of the droplet when aqueous droplets of poly(ethylene oxide) evaporate following a boot-strapping process in which the contact line undergoes fast receding, driven by polymer precipitation. Here we map out the phase behaviour of a combined particle-polymer system, illustrating a range of final deposit shapes, from ring-stain to flat deposit to pillar. Deposit topologies are measured using profile images and stylus profilometery, and characterised using the skewness of the profile as a simple analytic method for quantifying the shapes: pillars produce positive skew, flat deposits have zero skew and ring-stains have a negative value. We also demonstrate that pillar formation can be disrupted using potassium sulphate salt solutions, which change the water from a good solvent to a theta-point solvent, consequently reducing the size of the polymer coils. This inhibits polymer crystallisation, interfering with the bootstrap process and ultimately preventing pillars from forming. Again, the deposit shapes are quantified using the skew parameter.

PACS. 47.55.D Drops and bubbles – 47.57.Ng Polymers and polymer solutions

1 Introduction

The work of Deegan at.al. [1] investigated the properties of the coffee ring-stain, commonly seen when suspension droplets are left to evaporate on a solid surface. They proposed a simple explanation for these deposits with just two requirements: firstly, the triple line at the edge of the droplet must remain pinned to the substrate throughout (nearly all of) the drying process, known as constant contact radius drying (CCR) [2]; secondly the evaporative flux over the droplet varies with radius r measured from the centre of the droplet and diverges at the contact line $r = R$ following a power law. These two requirements lead to an outward flow to replenish solvent loss at the contact line, which sweeps suspended material to the contact line where it is deposited as a ring stain. The size and shape of the deposit is robust over a range of experimental parameters and follows simple power-law predictions [3]. One of the aims of ongoing research into drying sessile droplets is to control and prevent the formation of the coffee-ring stain as many commercial processes require a uniform deposit. Several mechanisms have been observed to achieve this goal including: non-spherical particles [4], capillary forces [5]; Marangoni flow induced by surface tension gradients [6]; electrowetting [7]; using droplets smaller than a critical size [8] and heated substrates [9]. Many of these effects are summarised in a recent review [10].

Send offprint requests to:

In many cases, ring stains are also suppressed if the liquid in the droplet undergoes a phase-change during evaporation. For example, in drying droplets of both dextran[11] and bitumen [12] the contact line becomes pinned, a flexible glassy skin with fixed surface area forms and as evaporation continues the film buckles leaving a final deposit in the shape of a sombrero. In previous work we have shown that aqueous droplets of poly(ethylene oxide) (PEO), a polymer which crystallises rather than vitrifies, follows a different drying route. The liquid droplet is squeezed inwards by a constricting ring of crystallising polymer at the contact line which eventually lifts the remaining liquid from the surface, forming polymer pillars which may be taller than the original droplet [13–17]. An aesthetically similar observation is seen in freezing water droplets as the water expands as it solidifies, leading to cusped solid deposits [18]. Likewise, droplets of salt solutions do not typically form ring-stains due to modified wettability once salt crystals begin to precipitate [19].

Others have also studied the drying behaviour of PEO droplets. Mamalis et. al. [20] varied the molecular weight and substrate chemistry to highlight the role of interfacial friction on pillar formation. Hu et.al. [21] placed 5% concentration droplets of 280,000 molecular weight PEO on both isothermal and heated substrates and found evidence for Marangoni flow at higher temperatures. Choi et.al. [22] added 1μm and 6μm hollow glass spheres to very dilute (maximum of 0.1%) PEO solutions with molecular weight

200,000 and 900,000 in order to alter the viscous drag on the moving particles. They found that even at such low concentrations, the effect of the polymer was sufficient to disrupt formation of the ring-stain.

The polymer used in this study is the very widely used linear polymer PEO, poly(ethylene oxide) [23–26]. It is unique amongst its homologues for its unusual solubility properties [27]: it dissolves in water, although at high concentrations or molecular weights, solutions can appear cloudy due to micron-sized clusters of undissolved polymer[28]. The origin of these clusters is still a point of contention[28]. The properties of PEO are very well known including data on its viscosity [29], solubility [30], phase behaviour [31] and crystallisation [32]. In water, PEO molecules adopt an expanded coil structure as water is considered a good solvent for PEO. The solvent quality can be reduced by adding salts which disrupt the water structure, reducing the favourable interaction between monomers and solvent until the theta point is reached, where the molecule is somewhat condensed and described by the statistics of an ideal coil. On the addition of further salt, the polymer will precipitate out of solution as it undergoes a coil-globule transition; several works have studied the effectiveness of various salts [33,34]. An interesting follow-up paper studied the change in polymer conformation using optical tweezers to show the elasticity of a single PEO molecule as the salt concentration is altered [35].

In this work we investigate two methods to control the pillar formation in aqueous PEO droplets. Firstly we study mixtures of PEO with polymer microparticles, mapping out how the droplet deposits change from ring-stain to pillars as the relative concentration of the two components are varied. We use two different sized particles and compare their effects. Secondly we disrupt the water structure by adding to the PEO solutions small quantities of the salt potassium sulphate, K_2SO_4, as this ranks relatively highly in both the Hoffmeister series (indicating a strong tendecy to induce protein precipitation) and in the data in Ref.[33] on the effect of various salts on PEO solubility. We study how the pillar formation is disrupted when the solvent quality is reduced leading to a reduction in the size of the dissolved polymer coil. To quantify our findings, we present a novel and versatile technique, using the skewness of a height profile, to distinguish quantitatively between the various deposits.

2 Methods

Polymer solutions were prepared by dissolving PEO powder (from Sigma Aldrich with average molecular weight M_W=100 kg.mol^{-1} and 200 kg.mol^{-1}) in distilled, deionized water with a range of mass concentrations c_0 and left to equilibrate for at least 24 hours. The particle suspensions used in this study were surfactant-free polystyrene spheres commercially available from Sigma-Aldrich with particle diameters of 500±50nm and 5±0.5μm, supplied at up to 10% solids by volume and a particle density of 1.050g.cm^{-3} at 20°C. The suspensions were used as supplied, then diluted with deionized water and added to the 100k PEO solutions to obtain samples with particle concentrations by mass c_P between 1% and 5 %. Due to the difficulties of dissolving PEO into the particle solutions, the highest polymer concentrations possible were around 16%. K_2SO_4 was added to other PEO solutions to give salt concentrations by mass c_S between 0.1% and 1.0%. As the salt comes in dry powdered form, it is possible to mix solutions with polymer concentrations as high as 25%. All samples were left on a SRT6-Stuart roller mixer for 12 hours to minimise the agglomeration of particles. The mixing process was repeated for at least 30 minutes prior to every experiment.

For the evaporation experiments, droplets of initial volume V_0 between 0.4μl and 5μl were slowly pipetted onto clean glass slides using a positive displacement Gilson pipette to ensure accurate dispensing of the viscous solutions. Previous work [14] has shown that provided the droplet dimensions are smaller than the capillary length (around 2mm), droplet volume does not affect deposition patterns. Samples were imaged from the side during drying using an Imaging Source CCD camera with IC Capture software, illuminated by a Stocker Yale diffuse back light (ML-045). ImageJ was used to analyse the images and extract the profile coordinates of the deposit from the images of the final deposit. Images of the final deposits were also taken using a Nikon Eclipse TE2000-S inverted microscope and an Olympus BX51 upright microscope using crossed-polarisers to highlight the crystallised polymer spherulites.

As some of the samples formed ring-stains, in which the centre was lower than the edge, images taken from the side were not able to capture the profile accurately. In these situations, the height profile of the deposits was analysed using a Dektat 150 surface profiler with a 1mg scan force to reduce the chance of damage to the delicate samples. The profiler recorded a line profile for each deposit with around 3μm horizontal resolution and almost 1nm vertical resolution. For each droplet, 6 scans were taken along diameters, spaced evenly around the deposit.

3 Results

Tables showing representative final images for the deposits, both profile and overhead, for both particle sizes and salt, are presented in Figs.1 to 6. The axes of the table for the salt samples have been transposed owing to the large number of difference concentrations used. Pillar formation, which is typically seen above 5% in pure PEO droplets, is shifted to higher concentrations with the addition of particles, with the 5μm particles in particular disrupting the pillars. Between 6% and 10% the pillars are more rounded and at their base extend the full width of the initial droplet. For all samples, steep, tall pillars are seen at high polymer concentrations. The disruption is less pronounced for the 500nm particles.

For samples with no polymer, the particle droplets show classic ring-stains and the salt solutions show the

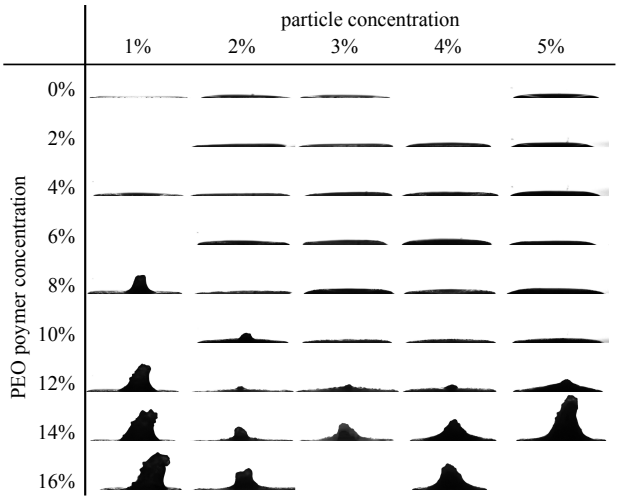

Fig. 1. Final profile images for 0.7μl droplets containing 100k PEO and 5μm particles with c_0 between 0% and 16% and c_p between 1% and 5%.

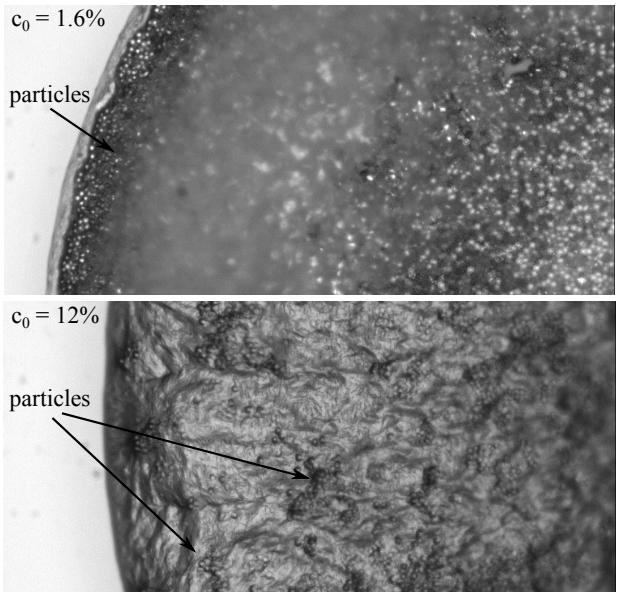

Fig. 2. Close-up images of the contact line of 0.4μl droplets with c_0 of 1.6% and 12% and concentration of 5μm particles c_p = 4%. At low c_0, particles are preferentially deposited at the edge, like a classic ring-stain despite the presence of polymer. At higher concentrations, the polymer disrupts the particle movement and consequently, particles are distributed more evenly.

more complicated crystal rings seen in such "creeping" solutions where the liquid spreads out over the deposited solid [19,36]. These deposits were also characterised using a stylus profilometer.

The overhead images of the droplets with 5μm particles are uniformly dark and did not reveal any particular variations between droplets, so are not included here. However, higher magnification microscopy close to the contact line shows that for low polymer concentrations, particles were deposited at the edge in a ring-stain, whereas

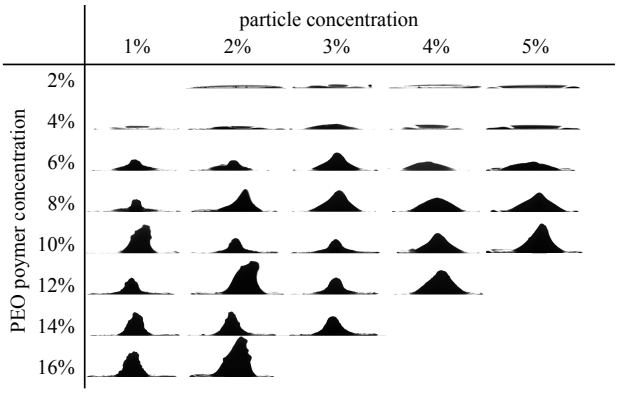

Fig. 3. Final profile images for 0.7μl droplets containing 100k PEO and 500nm particles with c_0 between 2% and 16% and c_p between 1% and 5% .

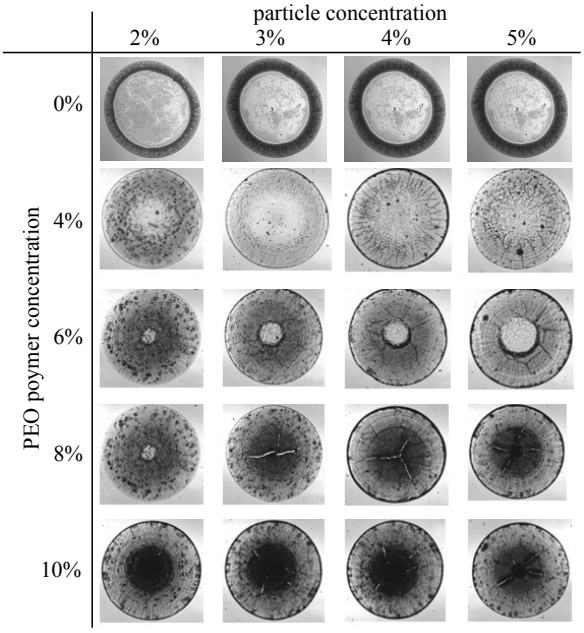

Fig. 4. Final overhead images taken through crossed polarisers of 0.4μl droplets containing 100k PEO and 500nm particles with c_0 between 0% and 10% and c_p between 2% and 5%. Ring-stains are clear at low values of c_0 and at higher values pillars are present, seen as a dark central circle in the images here with c_0 around 8% and above.

at higher c_0, particles were more evenly distributed, as illustrated in Fig.2.

The total drying time did not vary significantly between the various droplets and was around 600 seconds at standard atmospheric conditions.

The deposit shapes are more usefully quantified using surface profile data giving the height of the deposit $h(r)$ as a function of distance from the droplet centre r. As we have shown previously [3], robust ring-stains are observed over a range of experimental conditions, and here we confirm this result, finding clear ring-stains for all particle droplets without PEO, $c_0 = 0\%$, as evidenced by the $c_0 = 0\%$ curve in Fig.7 for 0.5μm particles. Note that there

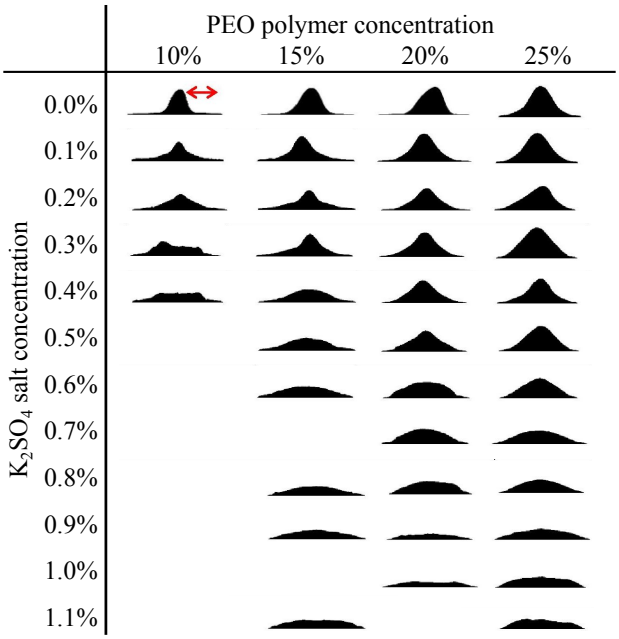

Fig. 5. Final profile images for 5μl droplets containing 200k PEO and K_2SO_4 with c_0 between 10% and 25% and c_S between 0% and 1.1%.

is at most a monolayer of particles deposited in the centre of the ring. The other curves in this figure show the effect of increasing PEO concentration: at low values of c_0, we still observe a ring-stain however with non-zero height in the centre. Fig 2 suggests that there may be separation between particles and polymer, as the ring preferentially contains particles, and the centre contains polymer. For higher concentrations, $c_0 \geq 7.2\%$, a central pillar is clearly defined, which increases in height with polymer concentration. The measured profiles using 5μm particles are not presented, but show a similar transition from ring-stain to pillar on the addition of PEO.

4 Discussion

We have shown qualitatively in the previous section that the addition of either particles or salt can disrupt the formation of PEO polymer pillars more dramatically than just considering the overall decrease in polymer concentration. In order to quantify how the shape of the deposits are altered we chose to measure the skewness γ_1 of the droplet profile. Skewness, which is related to the third moment of a distribution (as mean is related to the first moment and standard deviation to the second moment), indicates whether a distribution function leans to the left or right. As illustrated in Fig.7, this parameter distinguishes the three main types of pillar deposit: profiles which are peaked towards $r = 0$ have a positive skewness; ring-stain deposits in which the profile is peaked towards the edge at $r = R$ have a corresponding negative skew; and symmetrical flat deposits have a skewness close to zero. The simpler approach of using the value of r at which

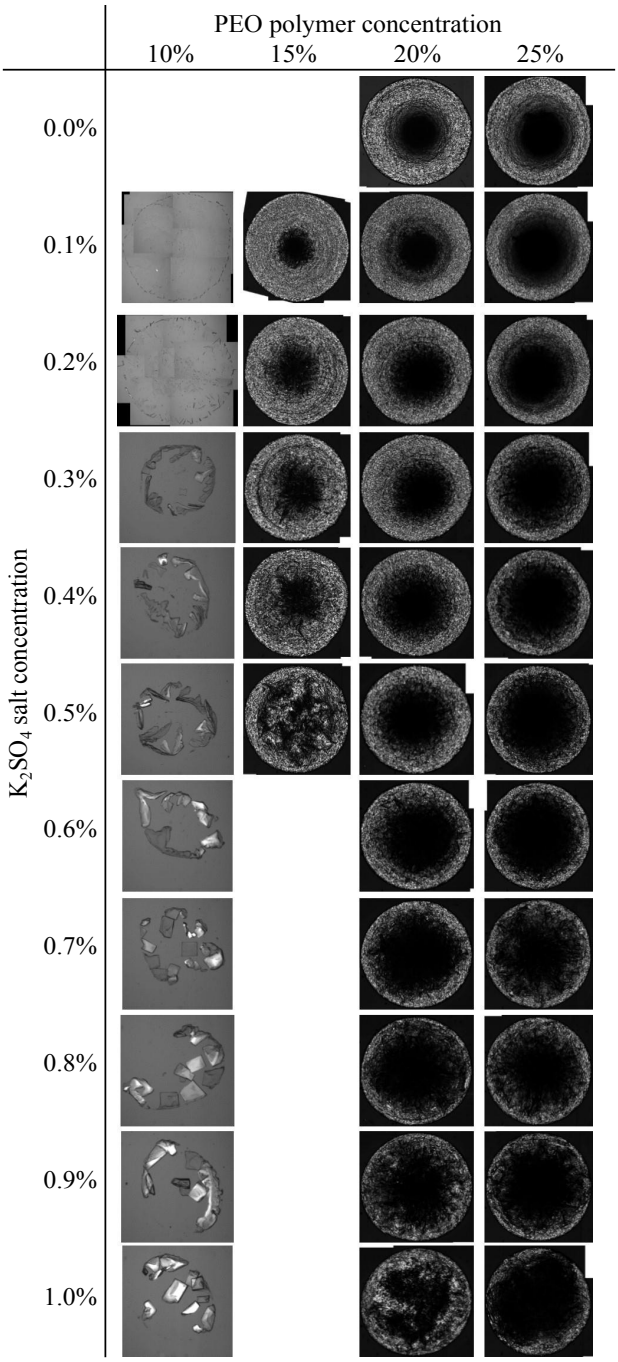

Fig. 6. Final overhead images taken through crossed polarisers for 5μl droplets containing 200k PEO and K_2SO_4 with c_0 between 10% and 25% and c_S between 0% and 1.0%.

the droplet height $h(r)$ is a maximum does not have to take into account the size of the peak, and therefore fails to consistently identify flattish deposits, where the maximum is not clearly defined. The use of skewness overcomes this problem.

The simplest definition of skew is the nonparametric skew, defined as the difference between the median and the mean $\bar{r}$ of the distribution, divided by the standard deviation. However, this approach did not reliably capture

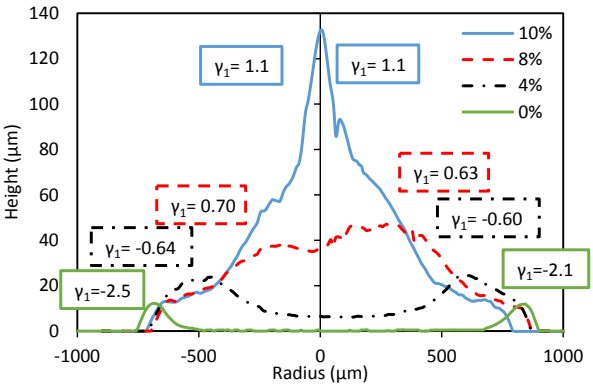

Fig. 7. Deposit profiles for 0.4μl droplets with polymer concentration c_0 between 0% and 10% and concentration of 0.5μm particles fixed at $c_\mathrm{p} = 4\%$. The values of the skewness γ_1 for both left and right sides of each profile are also indicated on the figure. With no polymer, $c_0 = 0\%$, the profile of a classic ring-stain is seen, with negative skewness $\gamma_1 < -2$. For $c_0 = 4\%$ a ring-like deposit at the edge is seen, with additional deposit in the centre and $\gamma_1 \approx -0.6$. For $c_0 = 8\%$, the deposit is a short pillar with $\gamma_1 \approx 0.66$ and for $c_0 = 10\%$ a tall pillar is seen with $\gamma = 1.1$

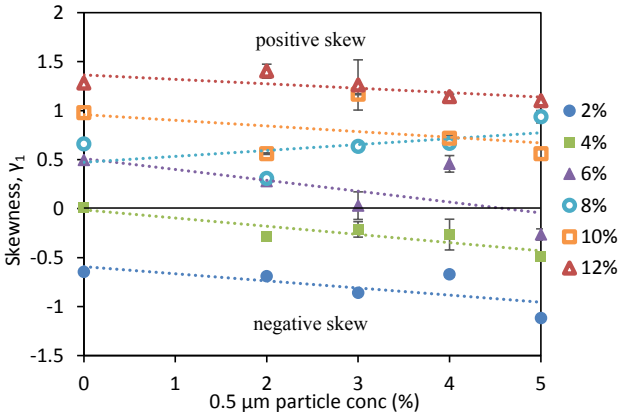

Fig. 8. Skewness of final deposit as a function of added concentration of 0.5μm particles into 0.7μl droplets containing 100k PEO at various concentrations. Vertical error bars indicate the difference in skew between the two sides, average over three droplets. Uncertainties in PEO concentration are around 0.5%

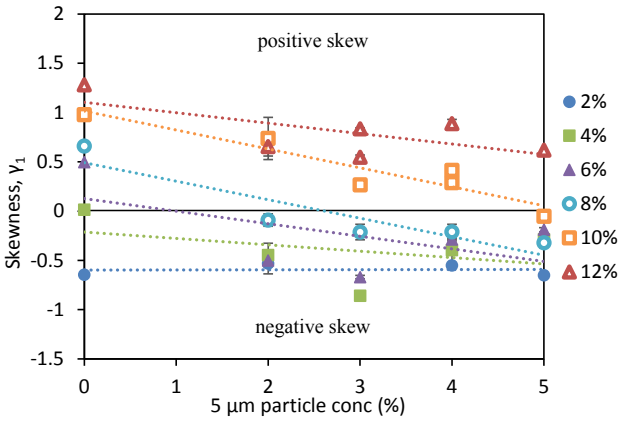

Fig. 9. Skewness of final deposit as a function of added concentration of 5μm particles into 0.7μl droplets containing 100k PEO at various concentrations. Vertical error bars indicate the difference in skew between the two sides, averaged over three droplets. Uncertainties in PEO concentration are around 0.5%.

the shape of the distributions, so for our analysis we used the standardised third moment of the radial profile. As the data obtained from both image analysis of the interface and surface profilometery is discrete with values of r_i, h_i (and an increment $\delta_i = r_{i+1} - r_i$ to account for data that are not necessarily equally spaced), we used the following formulae to calculate the skew:

$$\gamma_1 = \frac{\sum (r_i - \bar{r})^3 \, h_i \delta_i}{[\sum (r_i - \bar{r})^2 h_i \delta_i]^{3/2}}$$

For a given distribution, with r ranging from $-R$ to $+R$ we calculated the average of γ_1 for $0 < r < R$ for the right-hand side and $-\gamma_1$ for $-R < r < 0$ for the left hand side, the difference between the two halves characterising the uncertainty in the skewness.

The results for the skew analysis for all three systems are shown in Figs 8–10, with lines of best fit added for each value of c_0. Nearly all data sets show that the skewness of the deposit reduces with increasing additives, indicating that pillars become flatter. For the PEO plus particle droplets, the skewness becomes negative, indicating that the deposits have become ring-stains. However, the effect of adding particles is weak compared to the influence of polymer concentration in these samples. We calculate a *disruption factor* to quantify this effect, equal to the negative of the slope of the best-fit lines. These are plotted in the inset to Fig.10 and emphasise that only a small quantity of salt is required to prevent pillar formation. Presumably this is because the salt causes a molecular change to the PEO coils, hindering crystallisation, whereas the particles only cause a steric effect by physically obstructing the pillar formation process. The disruption factors for the polymer plus particle systems are significantly less, but even between these two, the 0.5μm particles seem to have less of an effect on the pillar formation process than the 5μm particles.

5 Conclusions

We have investigated the effect of adding two different sizes of micro-particles to evaporating droplets of poly(ethylene oxide) solution. In pure solutions, PEO forms tall pillars above around 5% concentration and micro-particles typically leave ring-stain deposits. By mixing polymer and particles we show that pillar formation is shifted to higher polymer concentrations when large 5μm particles are added, but is less affected by the addition of 500nm particles. We also show preliminary evidence for particle segregation at higher polymer concentrations. This observation opens up the possibility of using PEO pillars to create functional pillars containing bespoke particles. Potassium

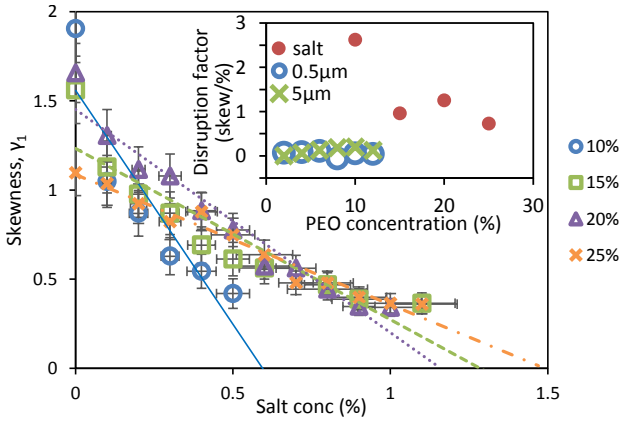

Fig. 10. Skewness of final deposit as a function of added concentration of K_2SO_4 salt to droplets containing 200k PEO at various concentrations. Vertical error bars indicate the standard deviation of skewness measured over 8 droplets. Uncertainties in PEO concentration are around 0.5%. The inset shows the disruption factor for each of the three systems as a function of PEO concentration.

sulfate is known to reduce the affinity of PEO with water, causing the coils to collapse. By adding this salt to evaporating PEO droplets we see significant interference of the pillar formation. To quantify the different deposits observed we introduce the use of the normalised third moment of the deposit profile, commonly known as the skewness. We show that this simple parameter seems to capture the three deposit types, with a positive skewness for pillars, close to zero for flat deposits and negative skewness for ring-stains. We believe skewness has the potential to be very useful for characterisation of deposits in a wide variety of systems.

6 Acknowledgements

Y. Msambwa is funded by the Tanzanian government through the Dar Es Salaam University College of Education. D.J. Fairhurst would like to thank NTU for funding a research sabbatical. We also acknowledge useful discussions initiated through COST Action MP1106.

References

1. RD Deegan, O Bakajin, TF Dupont, G Huber, SR Nagel, and TA Witten. Capillary flow as the cause of ring stains from dried liquid drops. *Nature*, 389(6653):827–829, Oct 23 1997.
2. R. G. Picknett and R. Bexon. The evaporation of sessile or pendant drops in still air. *Journal of Colloids and Interface Science*, 61:336–350, 1977.
3. Yohana Msambwa, David J Fairhurst, and Fouzia Ouali. How robust is the ring stain for evaporating suspension droplets? *Interfacial Phenomena and Heat Transfer*, 1(3), 2013.
4. Peter J Yunker, Tim Still, Matthew A Lohr, and AG Yodh. Suppression of the coffee-ring effect by shape-dependent capillary interactions. *Nature*, 476:308–311, 18 August 2011.
5. B. M. Weon and J. H. Je. Capillary force repels coffee-ring effect. *Physical Review E*, 82(1):015305, 2010.
6. H Hu and R G Larson. Evaporation of a sessile droplet on a substrate. *Journal of Physical Chemistry B*, 106(6):1334–1344, JAN 18 2002.
7. H. B. Eral, D. Mampallil Augustine, M. H. G. Duits, and F. Mugele. Suppressing the coffee stain effect: how to control colloidal self-assembly in evaporating drops using electrowetting. *Soft Matter*, 7:4954–4958, 2011.
8. X. Shen, C. M. Ho, and T. S. Wong. Minimal size of coffee ring structure. *The Journal of Physical Chemistry B*, 114(16):5269–5274, 2010.
9. Yanshen Li, Cunjing Lv, Zhaohan Li, David Quéré, and Quanshui Zheng. From coffee rings to coffee eyes. *Soft Matter*, 2015.
10. Khellil Sefiane. Patterns from drying drops. *Advances in Colloid and Interface Science*, (0), 2013. in press, http://dx.doi.org/10.1016/j.cis.2013.05.002.
11. L Pauchard and C Allain. Buckling instability induced by polymer solution drying. *Europhysics Letters*, 62(6):897–903, JUN 2003.
12. M. A. Rodríguez-Valverde, P Ramón-Torregrosa, A Páez-Dueñas, M. A. Cabrerizo-Vílchez, and R Hidalgo-Álvarez. Imaging techniques applied to characterize bitumen and bituminous emulsions. *Advances in colloid and interface science*, 136(1):93–108, 2008.
13. David Willmer, Kyle Anthony Baldwin, Charles Kwartnik, and David John Fairhurst. Growth of solid conical structures during multistage drying of sessile poly(ethylene oxide) droplets. *Physical Chemistry Chemical Physics*, 12(16):3998–4004, 2010.
14. Kyle Anthony Baldwin, Manon Granjard, David I. Willmer, Khellil Sefiane, and David John Fairhurst. Drying and deposition of poly(ethylene oxide) droplets determined by peclet number. *Soft Matter*, 7:7819–7826, 2011.
15. Kyle A Baldwin, Samuel Roest, David J Fairhurst, Khellil Sefiane, and Martin ER Shanahan. Monolith formation and ring-stain suppression in low-pressure evaporation of poly (ethylene oxide) droplets. *J. Fluid Mech.*, 695:321–329, 2012.
16. Kyle Anthony Baldwin and David John Fairhurst. Classifying dynamic contact line modes in drying drops. *Soft matter*, 2015.
17. K. A. Baldwin and D. J. Fairhurst. The effects of molecular weight, evaporation rate and polymer concentration on pillar formation in drying poly(ethylene oxide) droplets. *Colloid. Surface. A*, 441:867–871, 2014.
18. Alvaro G Marin, Oscar R Enriquez, Philippe Brunet, Pierre Colinet, and Jacco H Snoeijer. Universality of tip singularity formation in freezing water drops. *Physical review letters*, 113(5):054301, 2014.
19. D.J. Fairhurst. Droplets of ionic solutions. chapter 20. 2015.
20. Dimitrios Mamalis, Vasileios Koutsos, Khellil Sefiane, Antonia Kagkoura, Michail Kalloudis, and Martin ER Shanahan. Effect of poly (ethylene oxide) molecular weight on the pinning and pillar formation of evaporating sessile droplets: The role of the interface. *Langmuir*, 2015.

21. Yin-Chun Hu, Qiong Zhou, Hai-Mu Ye, Yu-Feng Wang, and Li-Shan Cui. Peculiar surface profile of poly (ethylene oxide) film with ring-like nucleation distribution induced by marangoni flow effect. *Colloids and Surfaces A: Physicochemical and Engineering Aspects*, 428:39–46, 2013.
22. Yongjoon Choi, Jeongin Han, and Chongyoup Kim. Pattern formation in drying of particle-laden sessile drops of polymer solutions on solid substrates. *Korean Journal of Chemical Engineering*, 28(11):2130–2136, 2011.
23. L Wallstronm and KAH Lindberg. Wood surface stabilization with polyethyleneglycol, peg. *Wood Science and Technology*, 29(2):109–119, FEB 1995.
24. A A Collyer. Turbulence and drag reduction: a macroscopic view (education). *Physics Education*, 10(4):305, 1975.
25. Andre C. Dumetz, Rachael A. Lewus, Abraham M. Lenhoff, and Eric W. Kaler. Effects of ammonium sulfate and sodium chloride concentration on peg/protein liquid-liquid phase separation. *Langmuir*, 24(18):10345–10351, SEP 16 2008.
26. A Abuchowski, T Vanes, NC Palczuk, and FF Davis. Alteration of immunological properties of bovine serum-albumin by covalent attachment of polyethylene-glycol. *Journal of Biological Chemistry*, 252(11):3578–3581, 1977.
27. Boualem Hammouda. Solvation characteristics of a model water-soluble polymer. *Journal of Polymer Science Part B - Polymer Physics*, 44(22):3195–3199, NOV 15 2006.
28. B Hammouda, DL Ho, and S Kline. Insight into clustering in poly(ethylene oxide) solutions. *Macromolecules*, 37(18):6932–6937, SEP 7 2004.
29. M Mohsen-Nia, H Modarress, and H Rasa. Measurement and modeling of density, kinematic viscosity, and refractive index for poly (ethylene glycol) aqueous solution at different temperatures. *Journal of Chemical & Engineering Data*, 50(5):1662–1666, 2005.
30. Stefan Bekiranov, Robijn Bruinsma, and Philip Pincus. Solution behavior of polyethylene oxide in water as a function of temperature and pressure. *Physical Review E*, 55(1):577, 1997.
31. Ana Saraiva, Ole Persson, and Aage Fredenslund. An experimental investigation of cloud-point curves for the poly (ethylene glycol)/water system at varying molecular weight distributions. *Fluid phase equilibria*, 91(2):291–311, 1993.
32. Ni Ding and Eric J Amis. Kinetics of poly (ethylene oxide) crystallization from solution: Temperature and molecular weight dependence. *Macromolecules*, 24(13):3906–3914, 1991.
33. F. E. Bailey Jr and R. W. Callard. Some properties of poly(ethylene oxide) in aqueous solution. *Journal of Applied Polymer Science*, 1(1):56–62, 1959.
34. Ebba Florin, Roland Kjellander, and Jan Christer Eriksson. Salt effects on the cloud point of the poly (ethylene oxide)+ water system. *Journal of the Chemical Society, Faraday Transactions 1: Physical Chemistry in Condensed Phases*, 80(11):2889–2910, 1984.
35. A. Dittmore, D. B. McIntosh, S. Halliday, and O. A. Saleh. Single-molecule elasticity measurements of the onset of excluded volume in poly (ethylene glycol). *Physical Review Letters*, 107(14):148301, 2011.
36. Willem JP van Enckevort and Jan H Los. On the creeping of saturated salt solutions. *Crystal Growth & Design*, 13(5):1838–1848, 2013.